Improving grid connected hybrid generation system using an adaptive super-twisting sliding mode and predictive current control strategy

Ridha Benadli*, Brahim Khiari, Anis Sellami*****

** National Higher Engineering School of Tunis, B.P 56, Bab Menara, Tunisia (Tel: 00216 97485127; e-mail: ridhabenadly@gmail.com).*
*** LaNSER Laboratory, CRTEn, BP: 95, Hammam-Lif 2050, Tunisia (e-mail: brahim.khiari@crten.rnrt.tn)*
**** National Higher Engineering School of Tunis, Tunisia, (e-mail: anis.sellami@esstt.rnu.tn)*

Abstract: In this paper, we proposed a new hybrid control structure that combines predictive current control (PCC) and adaptive super-twisting sliding mode control algorithm (STA). This structure, called super-twisting algorithm predictive current control (STA-PCC), was introduced for a three-phase voltage source converter (VSC) connected to the grid. The VSC was interfaced with two renewable energy systems (Photovoltaic (PV), Wind Turbine (WT)) and Battery Energy Storage System (BESS) to satisfy the energy needs of a micro-grid. Then, the STA-PCC was applied to the VSC to regulate the DC bus voltage and current for the purpose of enhancing dynamic tracking behavior of the power and improving the quality of the energy of the hybrid renewable energy system (HRES). Innovative control was also developed for DC-DC boost converter to maximize the available energy of the permanent magnet synchronous generator (PMSG) and that of bi-directional DC-DC converter in order to provide BESS with the necessary incoming power. In addition, the performance of the STA-PCC method suggested for the VSC was compared with that of the classical controls such as standard Proportional Integral (PI)–PCC control, first order PWM (Pulse-With Modulation) sliding mode control (SMC), Hysteresis Current Control (HCC), Voltage Oriented Control (VOC) and the traditional Direct Power Control (DPC). Many strategies were introduced to control the converters and validated by simulation using Matlab/SIMULINK. Obviously, VSC target control is more reliable than the conventional techniques in terms of reference tracking, energy quality and dynamic performance.

Keywords: predictive current control, adaptive super-twisting algorithm, hybrid renewable energy system, battery energy storage system, grid connected, voltage source converter.

1. INTRODUCTION

Renewable energies such as solar, wind, hydro, water, organic and other energies, will be increasingly used in the future because its non-polluting character to the environment. There is also pressing need for increased exploitation of renewable energy sources (RES) since demand for energy is rising rapidly, oil costs are augmenting, oil stocks are falling and climate changes considerable, which in turn leads to naturel disasters. In this context, the hybrid PV-Wind systems become more available and reliable than systems based on signal source (Chen, 2007). Moreover, the BESS can be combined with the (RES) connected to the power grid, which may reduce vulnerability to natural disasters (Bae, 2012) and guarantee more stable and reliable power supply (Rezvani, 2016).

In the literature (Chen, 2007; Seul-Ki; Kim 2008; Haque, 2008; Bae, 2012), numerous kinds of power converters were used with RES and BESS to develop HRES connected to the grid. Among these converters, the boost converter and the buck-boost converter are the most widely employed in this application for managing energy flow of the hybrid system. The boost converter is ordinarily utilized to guarantee the most extreme energy of the RES generator (Haque, 2008). The bi-directional buck-boost DC-DC converter controller is used to balance the power flow between the RES and the grid side (Bouharchouche, 2013). Moreover, the proportional-integral (PI) controller is the most common control technique used for power converters thanks to its simplicity of construction (Bouharchouche, 2013; Boukettaya, 2014). Generally, the synthesis of a PI controller depends on the mathematical model of the converters which lowers the system performance and stability of the system. To avoid these non-linearity problems, some studies proposed a robust and efficient controllers, such as Predictive Control (PC), for these applications.

In the late decades, Predictive Control (PC) has turned into a very popular and attractive control device to enhance the system performance in different applications. As a modern current technique strategy, PC is the most broadly utilized as a part of the industry (Rodríguez, 2007) thanks to high robustness (Zhang, 2014), high dynamic response speed (Vazquez, 2017; Cortes, 2009), also easy inclusion of nonlinearities (Kouro, 2009) as well as its simple use (Chelladurai J, 2017) and easy application in multivariable systems (Vazquez, 2017). In fact, the use of PC in the field of power electronics and drives (Aguilera, 2015; Almer, 2013, Bouafassa 2014, Judewicz, 2016; Kim, 2014; Nauman, 2016, Panten, 2016) as well in RES applications, like WT (Song,

2013) and PV (Boukezata, 2016; Lekouagheta, 2018), is relatively recent. This technique is based on using of a dynamic model of the system in order to anticipate the future behavior of the controlled variables for each switching state of the converter. For a three-phase VSC, the PCC is formulated to select an optimal switching state which minimizes the cost function (Rodriguez, 2007).

The three-phase VSC is utilized to realize the required exchange power from the grid, while keeping the DC interface voltage steady, to deliver sinusoidal waveforms with low Total Harmonic Distortion (THD). Therefore, the performance of this converter depends to a great extent on the control strategy employed in the VSC. Numerous control procedures were proposed to improve VSC performance; they can be classified according to the nature of the used servo loops which can be either current or power. Indeed, two control techniques are usually utilized in the literature. The first is based on the current control loops VOC (Benadli, 2015; Kadri, 2011), while the second relies on the power control loops DPC (Larrinaga, 2007).

In the VOC structure, there are two cascade control loops: An external voltage loop, which ensures a constant DC bus voltage, and an internal current loop that regulates the output power of the VSC. The linear PI controllers with a modulation block are employed in this scheme because of their simplicity. However, this technique often needs extra coordinate transformations and requires a large ratio between the switching and grid fundamental frequency to model the VSC (Larrinaga, 2007). In addition, the application of linear control to a non-linear system results in poor dynamic performance and stability of the system. For the DPC control, it can directly defines the voltage vectors according to the power errors between the power references and the real power and it does not require the internal current control loops and the PWM modulator block. However, this method produces large power ripple and yields current harmonics of the VSC connected to grid.

The standard PI-PCC strategy is the most appropriate solution for control VSC that gives more rapid response and less power fluctuations, compared with the two conventional VOC and DPC methods (Larrinaga, 2007). The external DC bus voltage with PI controller are generally used to provide the amplitude reference of the current taken to control the active power flow among the grid and the DC bus. The reference current and the measured current are applied to the input of the internal control loop with PCC in order to select the optimal control vector minimizing the cost function. In this case, the synthesis of a PI controller is based on the modelling of the system as a transfer function. Subsequently, the performance of the system can easily be degraded with the presence of nonlinear effects and disturbances. In addition, the PI controllers in grid connected to HRES are incapable in attaining the desired control goals under a wide variation of working conditions, under applied non-linear load in the system as well as under quickly changing atmospheric conditions and power demand.

The SMC is known by its excellent dynamic response and robustness to external disturbances and uncertainties such as unknown variations in control variables and system parameters (Scoltock, 2015; Héctor Huerta, 2018). Although the SMC-PCC is employed to improve both dynamic and stable performance of system, the application of this method may result in chattering phenomenon due to the oscillations appearing around the switching surface, which limits the use of this control (Utkin, 2009). At this stage, the STA strategy (Shtessel, 2012; Akshaya, 2017) represents an alternative to eliminate the chattering and preserve the accuracy and robustness of the control. In order to overcome these drawbacks of the PCC strategy with traditional SMC or with linear classical controller like PI controller or IP controller (Larrinaga, 2007; Rodriguez, 2007; Rodriguez, 2013; Boukezata, 2016; Lekouagheta, 2018), a new hybrid control structure, based on combining PCC control and an adaptive super twisting sliding mode control (STA) is proposed. This structure is called STA-PCC technique. The major benefits of the designed STA-PCC control scheme are as listed below:

- The proposed STA-PCC for DC-link voltage control can eliminate the chattering problems of the conventional SMC-PCC method and reduce all overshoot and undershoot of PI-PCC, which minimizes the size of the DC bus capacitor as well as the number of the used BESS and increases its lifetime.
- The developed STA-PCC injects power into the grid with good tracking indexes and with low THD (less than 2%) which does not exceed the limit required by the standard value equal to 5% under non-linear load.
- The introduced STA-PCC can enhance the performance and stability of the HRES as well as the setting time response of the VSC under various operating conditions.

In this study, a non-linear control strategy based on PCC coupled with an optimal rotational speed estimation block using a model reference adaptive system observer model (MRAS) is developed to track the maximum wind power from a VSWT. The MRAS observer based on two models (Maiti, 2009) is suggested to acquire the exact data about PMSG speed for a PCC control WT system. A classical maximum power point tracking (MPPT) method relying on Incremental Conductance (InCond) (Seul-Ki Kim, 2008; Hong, 2013) is applied to extract the maximum power point of PV generator. In addition, to provide the required reference current of the BESS, a current control algorithm using PCC technique for a bidirectional DC-DC converter is proposed in this research study. The non-linear controls designed using PCC show the best performance of the control strategies in various operating points of the hybrid system (wind speed variation, solar irradiation variation and grid demand changes).

2. FRAMEWORK DESCRIPTION AND PROBLEM FORMULATION

The design of the proposed system associated HRES including two RES (PMSG based on VSWT, PV array) and energy storage devices system (BESS) is presented in Fig. 1. Every component in the bloc is interconnected through its power converter (DC-DC or AC-DC) controlled by its nearby control law and is associated with the common DC-link bus.

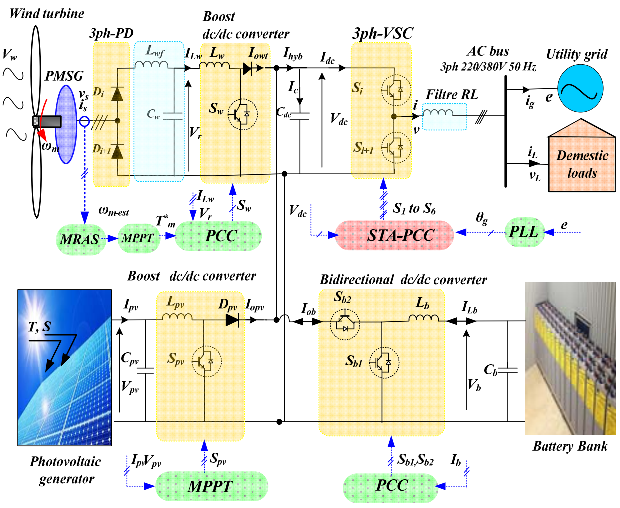

Fig. 1. Proposed design of the grid connected HRES.

The PV module used in the suggested system is SPR 305-WHT PV module (Saad, 2017). It is simulated by a single diode model with the corresponding electrical characteristics (Hong, 2013; Lekouagheta, 2018). To satisfy the energy demand of the DC bus, the power supplied with a single module is not sufficient. For this reason, we employed 5 modules connected in series and 5 modules connected in parallel to obtain a maximum power supplied by PV generator in the order of 7.625 kW in standard test conditions (STC). The output power-voltage-current characteristics, depending on the insolation *G* are presented in Fig. 2. The PV array is associated through a boost DC-DC converter for extracting the greatest power point MPP by utilizing MPPT method. A conventional MPPT technique based on Incremental Conductance (InCond) is utilized (Seul-Ki Kim, 2008; Hong, 2013) to ensure that the most extreme power is removed from the PV array and additionally to acquire a consistent DC bus voltage.

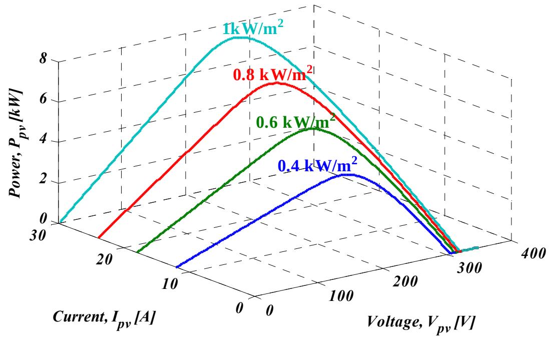

Fig. 2. Output characteristics produced by a PV array under various insolation *G* at steady *T* of 25 ºC.

The wind subsystem (6.kW) (Haque, 2008), including a turbine, is a little power wind equipped with a PMSG, a diode rectifier and a boost DC-DC converter to ensure the maximum power point (MPP) of this energy source. Fig. 3 shows the output characteristics generated by a turbine blades depending on the of rotation rotor speed at each wind speed, where the red curve represents the targets optimum characteristics.

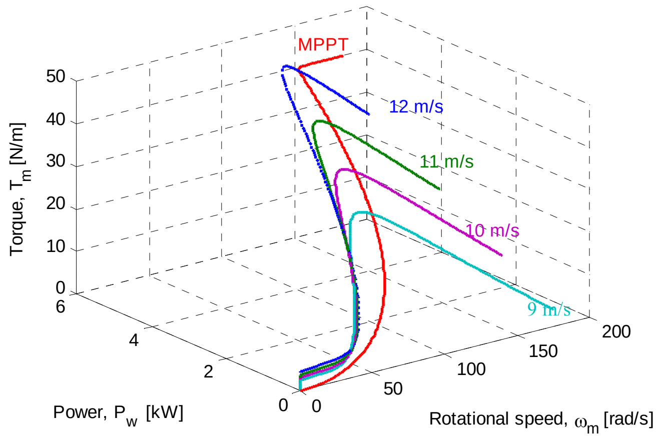

Fig. 3. Output characteristics produced by a WT system under different wind speeds.

An MPPT in perspective of PCC strategy is used for the boost DC-DC converter to expand the accessible vitality at VSWT. Hence, it is fundamental to acquire the average state-space model of the boost DC-DC converter. This average state-model model can be obtained by (Bouafassa, 2014)

$$\begin{cases} \dfrac{dI_w}{dt} = \dfrac{V_r}{L_w} - (1-d_w)\dfrac{V_{dc}}{L_w} \\ \dfrac{dV_{dc}}{dt} = (1-d_w)\dfrac{I_{Lw}}{C_{dc}} - \dfrac{I_{ow}}{C_{dc}} \end{cases} \tag{1}$$

where L_w, C_{dc}, d_w are electrical parameters of the boost converter, d_{fc} denote the duty cycle, V_r and I_{Lw} are respectively the input voltage and inductor current of the boost converter.

The lead-acid BESS is coupled with the assistance of (Tremblay, 2007, Rezvani, 2016) and it was employed in this work because it is the most popular due to law cost. The BESS is connected to the DC-bus through a DC-DC bi-directional buck-boost converter and the operating voltage is around 220 V. Besides, the linearized average state-space equations demonstrating the model of buck-boost bi-directional DC-DC converter related with the BESS is given by

$$\begin{cases} \dfrac{dI_{Lb}}{dt} = \dfrac{d_b}{L_b}V_b + (1-d_b)\dfrac{V_{dc}}{L_b} \\ \dfrac{dV_{dc}}{dt} = -\dfrac{(1-d_b)}{C_{dc}}I_{Lb} - \dfrac{I_{ob}}{C_{dc}} \end{cases} \tag{2}$$

where L_b, C_{dc} are electrical parameters of the buck-boost DC-DC converter, d_b denotes the duty cycle and I_{Lb} and I_{ob}

represent respectively the output current of the converter and the inductor current.

The grid-interface DC-AC converter transfers into grid DC power generation from the RES and BESS in the form of AC power. The VSC is essential in the HRES to regulate the power exchange among the BESS and the grid side according to grid demand variation and under changing atmospheric conditions while keeping a constant DC-link voltage. In order to attain the main goal of the VSC, it is necessary to obtain the mathematical model dynamics of this converter which can be obtained by applying the proposed STA-PCC in the α-β orthogonal coordinates and can be written as follows

$$\frac{di_{\alpha\beta}}{dt}=\frac{R}{L}i_{\alpha\beta}+\frac{1}{L}(v_{\alpha\beta-}e_{\alpha\beta}) \tag{3}$$

where $e_{\alpha\beta}$ and $i_{\alpha\beta}$ are respectively the grid voltage vectors and grid current vectors; $v_{\alpha\beta}$ corresponds to the voltage vectors generated by the VSC obtained by (Rodríguez, 2007)

$$V_{\alpha\beta}=V_{dc}S_{\alpha\beta} \tag{4}$$

where $S_{\alpha\beta}$ indicates the switching state vector of the VSC in the two-phase stationary α-β orthogonal coordinate.

On the other hand, the DC-link voltage can be expressed as follows

$$C_{dc}\frac{dV_{dc}}{dt}=I_{hyb}-I_{dc} \tag{5}$$

where C_{dc} stands for the DC-link capacitor voltage, I_{hyb} represents the output current of the HRES system and I_{dc} denotes the input current of the VSC.

For a balanced three-phase system, the instantaneous active and reactive output powers views, on the grid side in the rotating d–q frame can be defined as (Benadli, 2015)

$$\begin{cases} P_g=\frac{3}{2}\left(V_dI_d+V_qI_q\right) \\ Q_g=\frac{3}{2}\left(V_dI_q-V_qI_d\right) \end{cases} \tag{6}$$

Where V_d and V_q are respectively the d-q components of the output voltage; I_d, and I_q are corresponded respectively to the d-q components of the output current.

A phase locked loop (PLL) (Boukezata, 2016) was utilized to synchronize Park's transformation on the pulsation of the voltage measured on the grid. So, when the system was in a balanced three-phase system, the quadratic component V_q was set zero (Benadli, 2015). Therefore, the active and reactive power, can be represented by

$$\begin{cases} P_g=\frac{3}{2}V_dI_d \\ Q_g=\frac{3}{2}V_dI_q \end{cases} \tag{7}$$

The perfect VSC did not release losses and overheating, which made the power at the DC side relatively equivalent to the power at the VSC yield.

$$V_{dc}I_{dc}=\frac{3}{2}V_dI_d \tag{8}$$

Thus, we obtain

$$I_{dc}=\frac{3}{2}\frac{V_dI_d}{V_{dc}} \tag{9}$$

By putting (9) in (5), we have

$$I_{hyb}=C_{dc}\frac{dV_{dc}}{dt}+\frac{3}{2}\frac{V_dI_d}{V_{dc}} \tag{10}$$

Hence, the DC voltage can be written as follows

$$\frac{dV_{dc}}{dt}=\frac{1}{C_{dc}}\left(I_{hyb}-\frac{3V_dI_d}{2V_{dc}}\right) \tag{11}$$

3. CONTROL PROCEDURES OF HYBRID ENERGY SYSTEM

3.1. Proposed PCC for wind turbine system

Fig. 4 shows the structure of the introduced current control strategy of boost DC-DC converter which allows operating the WT at a maximum power point by acting on the duty cycle of switch (S_w).

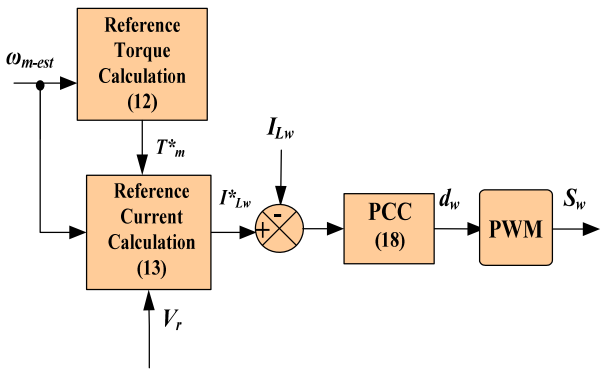

Fig. 4. Advanced control using PCC strategy for DC-DC boost converter related connected to WT source.

The reference torque was determined by estimating the generator speed ($\hat{\omega}_m$), as given by (Haque, 2008)

$$T_m^*=k_{opt}\left(\omega_{m-est}\right)^2 \tag{12}$$

where k_{opt} is a constant value, equals to 1.67×10^{-3} Nm/ (rad/s) determined by the WT characteristics.

The reference current was obtained by measuring the rectifier yield voltage (V_r), as given by

$$I_{Lw}^{*}=\left(\frac{T_{m}^{*}\omega_{m-est}}{V_{r}}\right) \tag{13}$$

In view of (2), the differential equation of the inductor current, can be expressed as

$$L_{w}\frac{dI_{Lw}(t)}{dt}=V_{r}(t)-(1-d_{w})V_{dc}(t) \tag{14}$$

The positive slope of inductor current**,** in the k^{th} switching cycle is $M_1(k)$ (*mode 1*: switch S_w is *OFF*), while the negative current value is $M_2(k)$ (*mode 2*: switch S_w is *ON*), as shown in Fig. 5. So, $M_1(k)$ and $M_2(k)$ can be written as follows

$$\begin{cases} M_{1}(k)=\dfrac{V_{r}(k)}{L_{w}} \\ M_{2}(k)=\dfrac{V_{r}(k)-V_{dc}(k)}{L_{w}} \end{cases} \tag{15}$$

Using (14) with a discrete time domain by applying forward-Euler discretisation (Scoltock, 2015), the inductor current at instant (k+1) is extended during a one switching period (T_s) and can be expressed as follows

$$I_{Lw}(k+1)=I_{Lw}(k)-M_{2}(k)(1-d_{w}(k))T_{s}+M_{1}(k)d_{w}(k)T_{s} \tag{16}$$

From (16), the duty cycle $d_w(k)$ can be deduced as

$$d_{w}(k)=T_{s}\frac{I_{Lw}(k+1)-I_{Lw}(k)+M_{2}(k)}{M_{2}(k)+M_{1}(k)} \tag{17}$$

Compensating $I_{Lw}(k+1)$ in (17) by the reference given in (13), the duty cycle can be expressed as

$$d_{w}(k)=T_{s}\frac{I_{Lw}^{*}-I_{Lw}(k)+M_{2}(k)}{M_{2}(k)+M_{1}(k)} \tag{18}$$

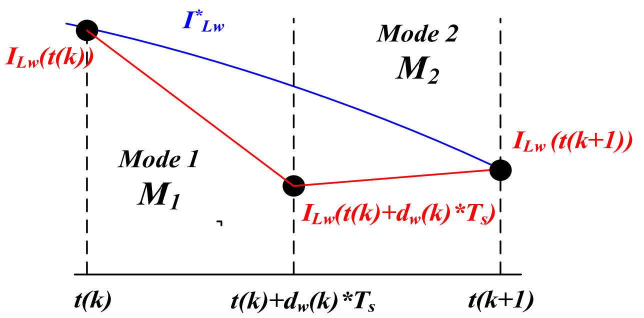

Fig. 5. Variation of inductor current during a one switching period.

3.2. Proposed PCC for BESS bi-directional dc-dc converter

The block diagram of the proposed control utilizing PCC method inside bi-directional DC-DC converter within a limit of the SOC (Bouharchouche, 2013) (0.5<SOC<0.8) is depicted in Fig. 6. The BESS can excess or inject the net power between the renewable energy sources (Wind, PV) and the demand power.

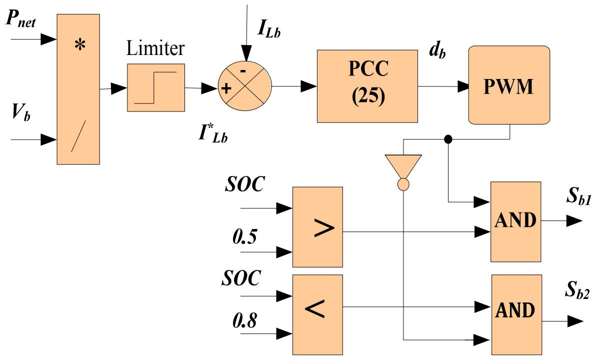

Fig. 6. Advanced control using PCC strategy for the bi-directional buck-boost converter.

In this study, the net power of the system is calculated as follows

$$P_{net}=(P_{pv}+P_{w})-P_{load} \tag{19}$$

where P_{pv} denotes the power created by the PV source, P_w indicates the power produced by the WT source and P_{load} represents the load demand power.

Considering (2), the differential equation of inductor current $i_L(t)$ in continuous time is written as follows

$$\frac{dI_{Lb}}{dt}=\frac{d_{b}}{L_{b}}V_{b}+(1-d_{b})\frac{V_{dc}}{L_{b}} \tag{20}$$

The positive slope of the inductor current in the k^{th} switching cycle is $N_1(k)$; whereas the negative current value is $N_2(k)$ (switch S_b is OFF). Thus, $N_1(k)$ and $N_2(k)$ can be written as shown below

$$\begin{cases} N_{1}(k)=\dfrac{V_{b}(k)}{L_{b}} \\ N_{2}(k)=\dfrac{V_{b}(k)+V_{dc}(k)}{L_{b}} \end{cases} \tag{21}$$

The discrete time of (20) becomes

$$I_{Lb}(k+1)=I_{Lb}(k)-N_{2}(k)(1-d_{b}(k)).T_{s}+N_{1}(k).d_{b}(k).T_{s} \tag{22}$$

Therefore, the duty cycle $d_b(k)$ is calculated as follows

$$d_{b}(k)=T_{s}\frac{I_{Lb}(k+1)-I_{Lb}(k)+N_{2}(k)}{N_{2}(k)+N_{1}(k)} \tag{23}$$

The main goal of applying the developed PCC for bi-directional DC-DC converter is to force the inductor current $I_{Lb}(k+1)$ to achieve the reference I_{Lb}^{*} given by

$$I_{Lb}^{*}=\frac{P_{net}}{V_{b}} \tag{24}$$

Compensating $I_{Lw}(k+1)$ in (22) by the reference given in (24), the duty cycle can be expressed as demonstrated in the following equation

$$d_b(k) = \frac{L_b}{T_s}\frac{I^*_{Lb} - I_{Lb}(k) + N_2}{N_2(k) + N_1(k)} \quad (25)$$

3.3. Proposed STA-PCC for VSC

The overall control diagram of the VSC using STA-PCC is depicted in Fig. 7. This control uses two cascaded independent control loops. The first one is an external loop relying on STA for controlling the DC link voltage, while the second one is an internal control loop based on PCC for controlling the currents in α-β synchronous reference frame. The DC link voltage regulation based on STA controller was employed to provide the d-axis reference current applied to control the active power transit between the grid side and the common DC bus. Based on (7), the desired active and reactive powers can be obtained by setting the d-q axis currents reference. The reference value of d-axis current (I^*_d) is estimated by STA controller. Moreover, the reference value of q-axis current (I^*_q) is imposed to zero in order to obtain the unity power condition (Benadli, 2015). The measured currents axis and its reference components in the d-q axis are transmitted to the internal control loop based on PCC method.

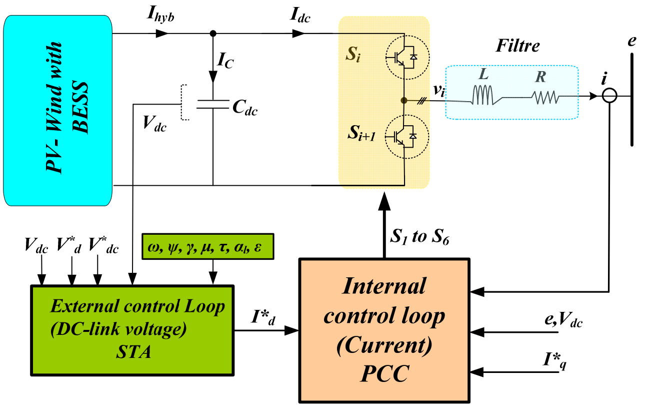

Fig. 7. Block diagram of the VSC connected to the grid with the proposed STA-PCC control scheme.

3.3.1 DC bus voltage regulation based on STA

The system model (11) can be written as a non-linear states-space equation in the following form:

$$\dot{x} = a(x) + b(x)u_i \quad (26)$$

where $x=V_{dc}$ represents the state variable and u_i denotes the control input.

We consider C, K_m, K_M, U_m and Q the arbitrary positive constants of the STA controller which are determined by considering the following condition of convergence given by (Akshaya, 2017)

$$|\dot{a}(x)| + U_m\left|\dot{b}(x)\right| \le C;\ k_m \le b(x) \le K_M; \left|\frac{a(x)}{b(x)}\right| < qM; 0 < q < 1$$

The main purpose of employing STA controller is to create a second-order sliding regime on the surface $s(x)$ by the cancelling $s(x)$ and its derivative $\dot{s}(x)$ in a limited time ($\dot{s}(x)$ = $s(x)=0$). The general form of the equation applied for the sliding surface is as follows (Slotine JJ, 1991)

$$s(x) = (\frac{\partial}{\partial t} + \lambda)^{(r-1)} e(x) \quad (27)$$

with $e(x)$ corresponds to the error between the controlled variable x and its reference x^* and r denotes the relative degree of the system. The STA controller is used in the system (11) with a relative degree equal to one. So, the sliding surface is defined in accordance with (27) as presented by

$$s(x) = x - x^* \quad (28)$$

In view of (26), the first derivative of $s(x)$ is calculated as follows

$$\dot{s}(x) = \left(a(x) + b(x)u_i\right) - \dot{x}^* \quad (29)$$

From (29), the $x^*=V^*_{dc}$ is a steady amount. Hence, its time derivative can be taken as zero

$$\dot{s}(x) = \left(a(x) + b(x)u_i\right) \quad (30)$$

The control unit of a STA controller is constructed by two terms. The first term is continuous sliding variable function (u_{eq}), while the second term is the discontinuous function (u_n). Thus, the general controller yield is given by (Utkin V, 2009)

$$u_i = u_n + u_{eq} \quad (31)$$

The equivalent control law (u_{eq}) is obtained by supposing that the time derivative of sliding surface is equal to zero ($\dot{s}(x)$ = 0) (Utkin V, 2009). According to (30), we can deduce its expression by

$$u_{eq} - b(x)^{-1} a(x) \quad (32)$$

We define u_n as follows

$$u_n = -b(x)^{-1} u_{st} \quad (33)$$

where u_{st} is the STA term defined by (Shtessel, 2012)

$$u_{st} = \left[-\alpha_a\sqrt{|s|}sign(s) - \beta_a \int sign(s)\right] \quad (34)$$

In this equation, α_a and β_a are the adaptive gains given by (Akshaya K, 2017)

$$\dot{\alpha}_a = \begin{cases} \omega\sqrt{\frac{\psi}{2}}sign\left(|s(x)| - \gamma\right) & \text{if } \alpha_a > \alpha_l \\ \mu & \text{if } \alpha_a < \alpha_l \end{cases} \quad (35)$$

$$\beta_a = \tau\alpha_a \quad (36)$$

where ω, ψ, γ, μ, τ, α_l and ε are the arbitrary positive constants.

Compensating u_i in (31) by I_d^*, the expression for the control law of STA controller is determined by

$$I_d^* = \left(\frac{2C_{dc}V_{dc}}{3V_d^*}\right)\left(\frac{I_{hyb}}{C_{dc}} + \alpha_a\sqrt{|s|}sign(s) + \int \beta_b.sign(s)dt\right) \quad (37)$$

where V_{d*} represents the reference value of the direct component voltage which considered constant equal to the amplitude of the balanced grid voltages.

Theorem. As per Lyapunov direct strategy (Utkin V, 2009) the Lyapunov function is picked as $V(s) = 0.5s^2 > 0, \forall\ s \neq 0$. A fundamental and adequate condition, for the nonlinear framework (11) with a control law STA (37) to uniting the sliding surface s (28) until zero, is that the derivative of $V(s)$ has to be negative $\dot{V}(s) = s\dot{s} < 0,\ \forall\ s \neq 0$. This inequality represents two characteristics, which are the stability and the robustness of the STA, to regulate the DC bus voltage for a steady reference despite the distinctive working states of the PV-Wind-BESS hybrid system.

Proof. Considering (28), (29) and (37), (29) becomes

$$\begin{aligned}\dot{s} &= \frac{1}{C_{dc}}\left(I_{hyb} - \frac{3V_d^* I_d^*}{2V_{dc}}\right) \\ &= -\alpha_a\sqrt{|s|}sign(s) - \int \beta_b.sign(s)dt\end{aligned} \quad (38)$$

Referring to (38), the time derivative of $V(s)$ can be written as

$$\dot{V}(s) = s\dot{s} = -s.sign(s)\left(\alpha_a |s|^{\frac{1}{2}} + \beta_a t\right) < 0 \quad (39)$$

Therefore, the stability of STA controller is verified through the Lyapunov condition provided by (39) which always gives an opposite sign since all coefficients have positive values. The block implementation diagram based on the proposed STA voltage regulation is appeared in Fig. 8.

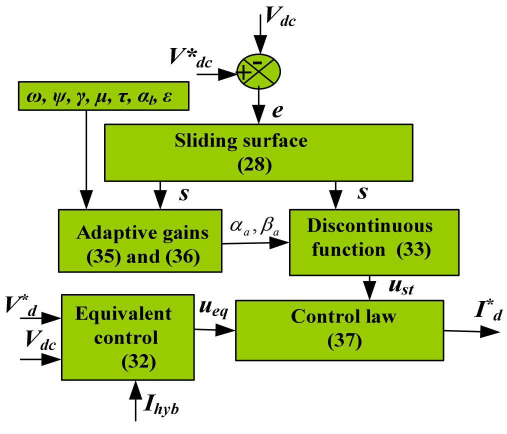

Fig. 8. Block diagram of the designed STA for DC-link voltage regulation.

3.3.2 Current regulation based on PCC

The implemented diagram of current regulation using PCC is depicted in Fig. 9. It consists of two main elements the discrete-time predictive model and the cost function (optimiser). The discrete-time predictive model is utilized to anticipate the behavior of the current $i^p_{\alpha\beta}(k+1)$ for all possible voltage vectors (V_j; j=0 to 7) generated by the VSC (Fig. 10). Then, the optimizer delivers a one optimum voltage vector to be applied at the input of the VSC during one switching period (T_s), which allows reducing the error between the predicted model of output current $i^p_{\alpha\beta}(k+1)$ and the reference current $i^*_{\alpha\beta}(k+1)$.

In this paper, a cost function *(g)* is applied to limit the errors between the reference current and the predicted current (Cortes 2012; Rodriguez, 2013; Boukezata, 2016).

$$g = \left|i_\alpha^*(k+1) - i_\alpha(k+1)\right| + \left|i_\beta^*(k+1) - i_\beta(k+1)\right| \quad (40)$$

where $i^*_\alpha(k+1)$ and $i^*_\beta(k+1)$ are respectively the real part and imaginary part of the reference current vector; $i_\alpha(k+1)$ and $i_\beta(k+1)$ correspond respectively to the real part and imaginary part of the predicted grid current vector.

For a short sampling period time (T_s), it can be supposed that $i^*_{\alpha\beta}(k+1) = i^*_{\alpha\beta}(k)$ (Rodriguez, 2007) and no extrapolation is required. The predicted yield current at instant $(k+1)$ is computed by utilizing a discrete-time model of the grid side VSC given by

$$i_{\alpha\beta}^p(k+1) = \left(1 - \frac{R}{L}T_s\right)i_{\alpha\beta}(k) + \frac{T_s}{L}\left(v_{\alpha\beta}(k) - e_{\alpha\beta}(k)\right) \quad (41)$$

where R and L are respectively the grid resistance and the grid inductance. The flow diagram chart of this control strategy is detailed in Fig. 11.

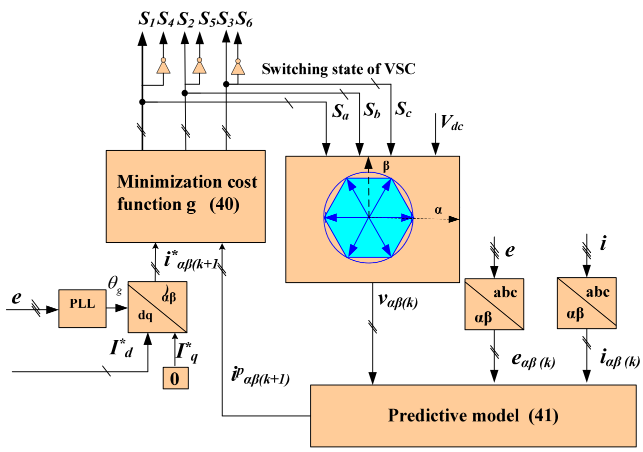

Fig. 9 Block diagram of the designed PCC for inner-loop current regulation.

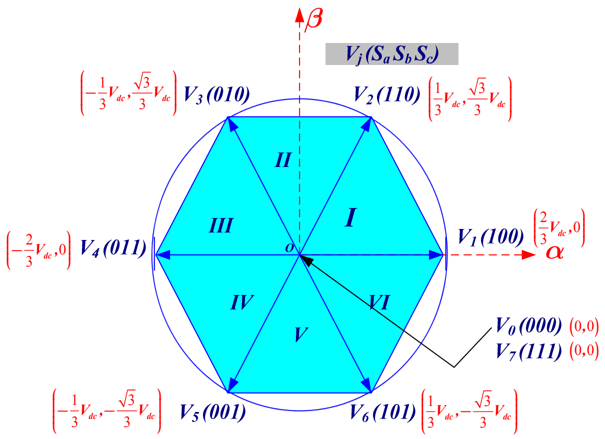

Fig. 10. Switching state (S_a, S_b, S_c) and components of each voltage vector (V_j; j=0 to7) in the α-β axis of VSC.

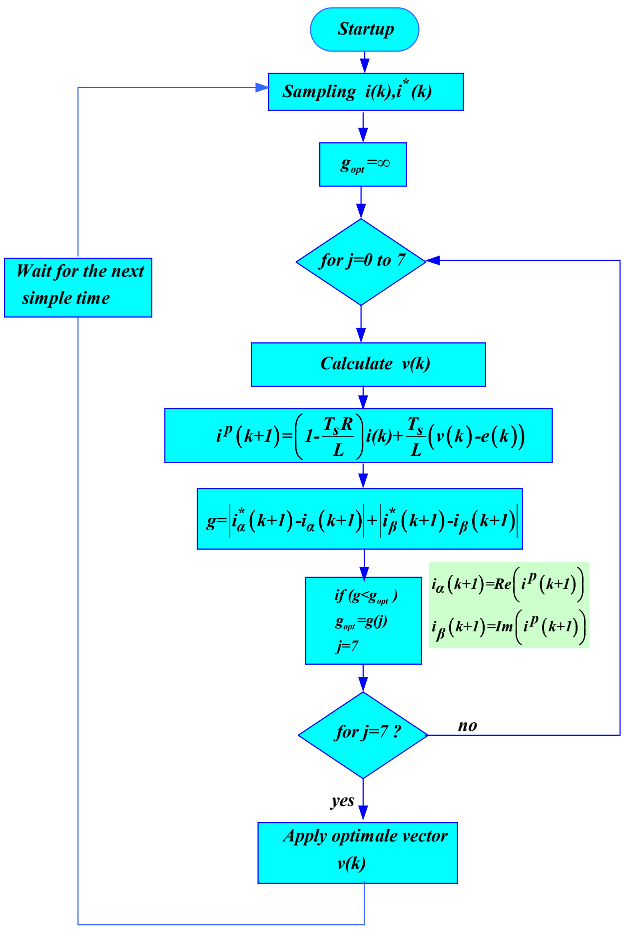

Fig. 11. Flow chart diagram based on PCC approach.

4. SIMULATION RESULTS

To examine the performance of the controllers applied in global HRES, which are connected to the grid presented in Fig. 1, simulation was executed by using MATLAB/Simulink environment. The essential parameters of the grid side VSC are mentioned in Appendix 1. The wind generator provided 6 kW maximum power under wind speed (V_ω) of 12 m/s while the PV generator delivered 7.625 kW maximum power under a STC. The first simulation section centered on the voltage tracking performance under a fixed power load demand (6 kW) and with a constant climatic condition (V_ω=12 m/s, G=1kW/m^2 and T=25 °C). Fig. 12 shows the comparison between the tracking performance of DC-link voltage and its zoomed figure with PI-PCC method, PWM first-order SMC-PCC method and the designed STA-PCC approach. The control law for the external control loop DC-link voltage based on PWM first order SMC is given by

$$I_d^* = I_{hyb}\left(\frac{2V_{dc}}{3V_d^*}\right) - k.sgin(s(x)) \tag{42}$$

where k is a positive constant gain.

It is observed, from Fig. 12, that the three techniques are able to follow the desired DC-link voltage, but the VSC controlled by the designed STA-PCC method gives a more tracking voltage performance than other conventional methods. The proposed control has a much faster tracking where the designed method took only 0.09s to reach the reference DC-link voltage, while the PI-PCC and SMC-PCC needed 0.16s and 0.15s respectively. Compared with the 3.79% overshoot on the DC-link voltage obtained by the conventional PI-PCC scheme, the overshoot on the DC-link voltage was reduced to 2.31% by applying STA-PCC method. On the other hand, the oscillations in voltage (chattering phenomenon) were clearly visible with the SMC-PCC, while they were eliminated by employing proposed control scheme. It can be noticed that the ability of the introduced STA-PCC for DC-link voltage control can avoid the chattering problems of the conventional SMC-PCC method and reduce the overshoot of PI-PCC, which minimizes the size of the DC bus capacitor as well as the number of the utilized BESS and expands its lifetime. Table 1, illustrates the comparison between the designed STA-PCC technique and the conventional methods in term of voltage tracking performance according numerous indicators such as overshoot (M_v), settling time (T_v) and mean study-state error (E_v). It can be deduced, from Table 1 that the greatest results of DC-link voltage tracking performance were obtained by the designed STA-PC scheme.

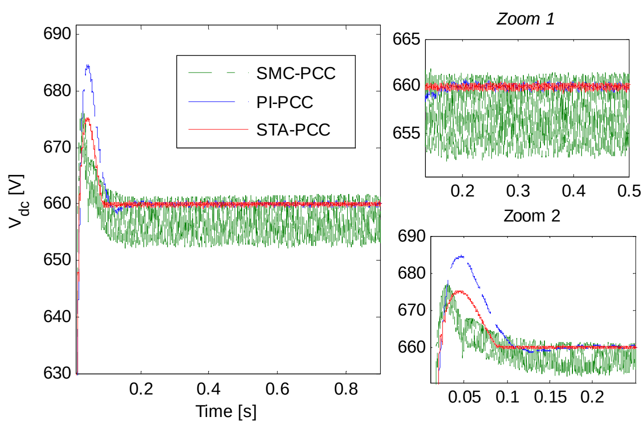

Fig. 12. DC-bus voltage regulation and its zoomed with the three applied methods.

Table 1. Summary of voltage tracking performance.

Method	T_v *(sec)*	M_v *(%)*	E_v *(V)*
STA-PCC	0.09	2.31	0.004
SMC-PCC	0.15	2.57	-6.52
PI-PCC	0.16	3.79	0.005

The second simulation section concentrated on the control of the HRES using the proposed method under various working conditions with variation in the insolation *G* of PV array, wind speed and load demand. The wind speed increased from 10 m/s to 12 m/s at t=1.2, while the insolation G rose from 0.8 kW/m^2 to 1kW/m^2 at t=0.75s and decreased from 1kW/m^2 to 0.9kW/m^2 at t=1.5s. The power load demand (P_{Load}) is augmented from 6 kW to 18 kW at t=1s. The performance of WT controller is demonstrated in Fig. 13. This figure shows the real speed and estimated speed of the PMSG based on the MRAS method, different torques output, the measured inductor current witch its reference, the power coefficient, the mechanical and electrical power). It is clear, from Fig. 13, that the proposed control was able to keep the WT source inside its optimal range imposed by the MPPT algorithm for the wind turbine.

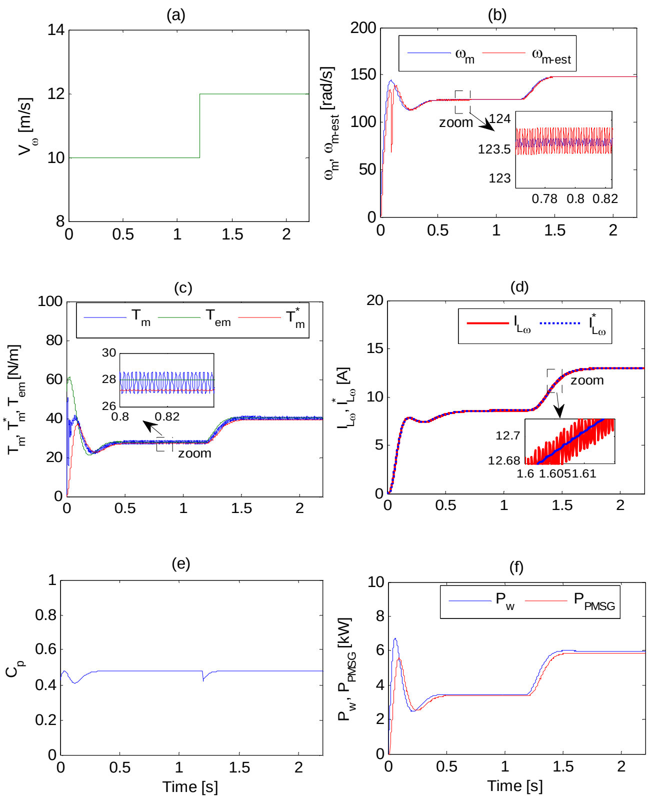

Fig. 13. Control performance of the WT system: (a) wind speed (V_w), (b) real speed (ω_m) and estimated speed (ω_{est}); (c) mechanical torque (T_m), reference torque (T^*_m) and generator electromagnetic torque (T_{em}); (d) measured current ($I_{L\omega}$) and reference current ($I^*_{L\omega}$); (e) power coefficient (C_p); (f) mechanical power from the WT system (P_m) and electrical power produced by the PMSG(P_{PMSG}).

The performance of BESS controller in term of inductor current, power, voltage and state of charge *(SOC)* is delineated in Fig. 14. Obviously, the proposed PCC solution allowed maintaining the power balance of the system.

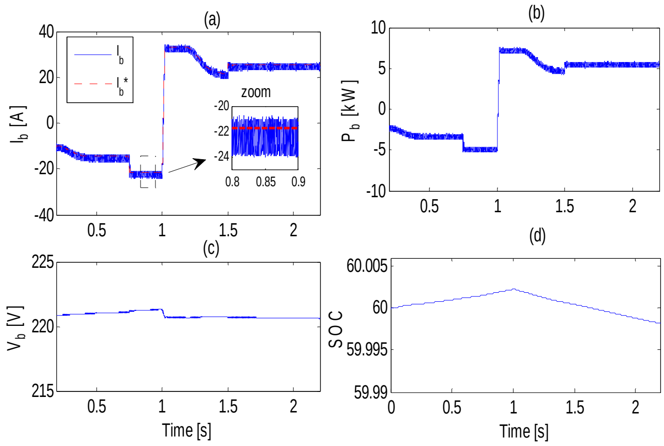

Fig. 14. Control performance of the BESS: (a) reference current (I^*_b) and battery current (I_b); (b) battery output power (P_b); (c) battery voltage (V_b); (d) state of charge (*SOC*).

The performance of VSC controlled by the proposed STA-PCC is shown in Fig.15 and Fig. 16. Fig. 15(a) demonstrates the distinctive yield powers of the proposed HRES. It can be seen, from Fig. 15 (b), that the DC-link voltage *(V_{dc})* tracks its reference voltage (660V) with excellent dynamic response exactness and stability. Fig. 16 (a) reveals that the phase current become in sinusoidal current is in phase with the grid voltage. It is obvious, from Fig. 16 (b), that the real part and imaginary part of the current vector follow the reference currents and the average error is approximately equal to zero.

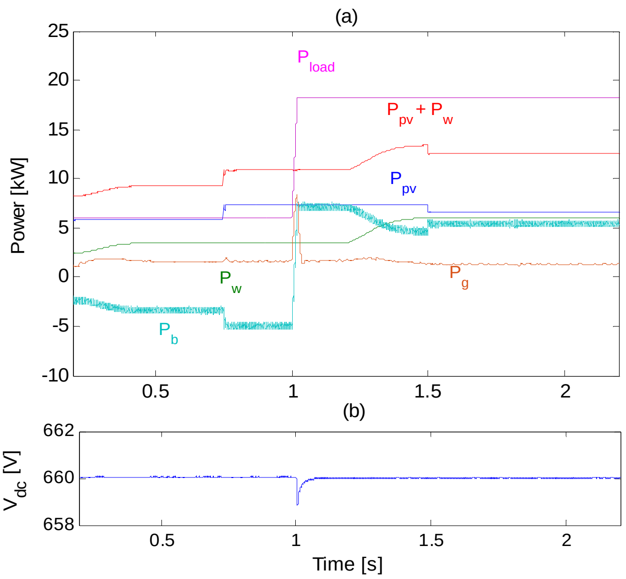

Fig. 15. Control performance of the VSC: (a) different output powers among different components of the hybrid system wind power (P_w), PV array power (P_{pv}), RES power source (P_{pv}+P_w), BESS power (P_b), load power (P_{load}) and the grid power; (b) DC-link voltage (V_{dc}).

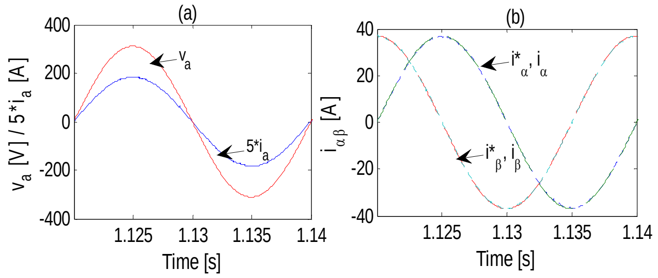

Fig. 16. Simulation results obtained using the proposed STA-PCC approach: (a) current and voltage curves; (b) measured currents with their references components in the α-β axis.

The third part of the simulation focused on the performance of VSC controller under a non-linear load connected to the grid side. The weather conditions were set at STC (V_w =12 m/s, G=1 kw/m^2 and T= 25 C). Keeping in mind that the end goal of our study is to demonstrate the capability of the proposed STA-PCC approach to enhance the system performance, a comparative simulation was made. In this simulation, we used the standard PI-PCC, the conventional SMC-PCC, the classical DPC (Larrinaga, 2007), the traditional HCC, the conventional VOC (Kadri, 2011) and the proposed STA-PCC. Initially, a resistive load with dynamic power rating of 4.5 kW was connected to the system and a non-linear load (three-stage diode rectifier combined with a resistive–inductive load) with dynamic power rating of 5.5 kW was connected to the system at time t =0.5s.

The transient responses of both active and reactive powers for ach technique under variation of load are displayed in Fig. 17.

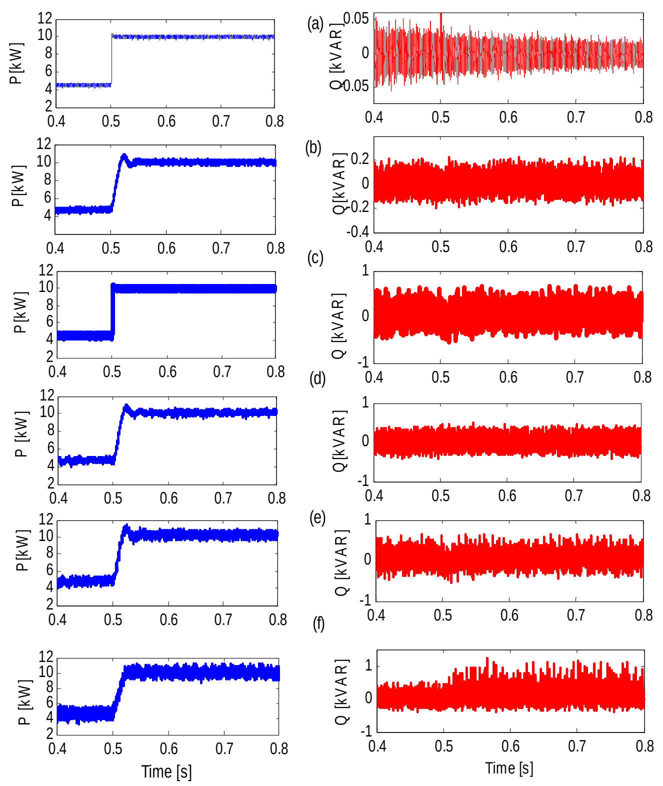

Fig. 17. Transient response of both dynamic active and reactive power using different control strategies: (a) the proposed STA-PCC approach, (b) the standard PI-PCC, (c) the traditional PWM first order SMC, (d) the classical HCC (e) the conventional VOC and (f) the conventional DPC.

It is clearly seen, from Fig. 17, that each active and reactive power instantaneous follows its reference with each method under load variation. Moreover, excellent transient responses with a high precision, and good stability were obtained by applying the introduced STA-PCC technique. In addition, the comparison of the performance of the developed STA-PCC approach with that of the traditional controls in term of tracking powers performance is given in Table 2. It is clearly from the comparison that the introduced STA-PCC technique has fastest dynamic response T_p (around 0.01 sec), the least overshoot M_p (about 0.022 %), the smallest mean error in active power E_p (less than 0.2 kW), the most inferior mean error in reactive power E_q (less than 0.05 kVAR) and lowest THD of current (less than 2%) compared to the other control methods. Finally, it can be concluded that the tracking powers performance and the THD of the suggested STA-PCC are better than those of the conventional techniques.

Table 2. Comparison of the performances of the VSC under load variation.

Method	T_p *(sec)*	M_p *(%)*	E_p *(kW)*	E_q *(kVAR)*	THD_i *(%)*
STA-PCC	0.01	0.022	< 0.2	< 0.05	1.72
PI-PCC	0.035	0.08	< 0.4	< 0.2	2.45
SMC-PCC	0.012	2.5	<1.5	< 1	3.15
HCC	0.054	0.1	< 0.5	< 0.5	3.44
VOC	0.055	0.13	< 0.5	< 0.5	9.91
DPC	0.052	0.01	< 1	< 1	8.93

5. CONCLUSION

In this paper, we suggested control scheme using STA-PCC strategy proposed for a grid connected to VSC linked to two RES (Wind, PV array) and BESS. Form the simulation results, it was obvious that the designed STA-PCC for the VSC provided a very satisfactory DC-link voltage tracking performance in terms of dynamic response, overshoot and steady state error, compared with PI-PCC and SMC-PCC techniques. The obtained findings also show that, with the same load variation, the proposed STA-PCC offered better tracking powers performance (fastest dynamic response, less overshoot, smaller mean error) with a high precision, and good stability than the five traditional control techniques. In fact, the ability of the proposed PCC methods to control the various converters incorporated into BESS and WT generator was demonstrated by extensive simulation studies. The efficiency and the THD of the system were greatly improved thanks to the advanced control strategy applied in the VSC. In addition, the developed controls ensured a stable operation of HRES under different operating conditions.

REFERENCES

Aguilera, R. P., and Quevedo, D. E. (2015). Predictive Control of Power Converters: Designs With Guaranteed Performance. *IEEE Transactions on Industrial Informatics*, 11(1), 53–63.

Akshaya K. Pati, N.C. Sahoo. (2017). Adaptive super-twisting sliding mode control for a three-phase single-stage grid-connected differential boost inverter based photovoltaic system. *ISA Transactions,* 69, 296-306.

Almer, S., Mariethoz, S., and Morari, M. (2013). Sampled Data Model Predictive Control of a Voltage Source Inverter for Reduced Harmonic Distortion. *IEEE Transactions on Control Systems Technology*, 21(5), 1907–1915.

Bae, S., and Kwasinski, A. (2012). Dynamic Modeling and Operation Strategy for a Microgrid With Wind and Photovoltaic Resources. *IEEE Transactions on Smart Grid*, 3(4), 1867–1876.

Benadli, R., Khiari, B., and Sellami, A. (2015). Three-phase grid-connected photovoltaic system with maximum power point tracking technique based on voltage-oriented control and using sliding mode controller. *The Sixth International Renewable Energy Congress*.

Bouafassa, A., Rahmani, L., Kessal, A., and Babes, B. (2014). Unity power factor Converter based on a Fuzzy controller and Predictive Input Current. *ISA Transactions*, 53(6), 1817–1821.

Bouharchouche, A., Berkouk, E. M., and Ghennam, T. (2013). Control and energy management of a grid connected hybrid energy system PV-wind with battery energy storage for residential applications. *2013 Eighth International Conference and Exhibition on Ecological Vehicles and Renewable Energies (EVER)*.

Boukettaya, G., and Krichen, L. (2014). A dynamic power management strategy of a grid connected hybrid generation system using wind, photovoltaic and Flywheel Energy Storage System in residential applications. *Energy*, 71, 148–159.

Boukezata, B., Gaubert, J.-P., Chaoui, A., and Hachemi, M. (2016). Predictive current control in multifunctional grid connected inverter interfaced by PV system. *Solar Energy*, 139, 130–141.

Chelladurai J, Vinod B, Joe Brislin J. (2017). Finite Control Set based Optimized Model Predictive Current Control of Fourleg Shunt Active Power Filter. *Control Engineering and Applied Informatic*, 19(1), 67-76.

Chen, Y.-M., Liu, Y.-C., Hung, S.-C., and Cheng, C.-S. (2007). Multi-Input Inverter for Grid-Connected Hybrid PV/Wind Power System. *IEEE Transactions on Power Electronics*, 22(3), 1070–1077.

Cortes, P., Ortiz, G., Yuz, J. I., Rodriguez, J., Vazquez, S., and Franquelo, L. G. (2009). Model Predictive Control of an Inverter With Output LCL Filter for UPS Applications. *IEEE Transactions on Industrial Electronics*, 56(6), 1875–1883.

Cortes, P., Rodriguez, J., Silva, C., and Flores, A. (2012). Delay Compensation in Model Predictive Current Control of a Three-Phase Inverter. *IEEE Transactions on Industrial Electronics*, 59(2), 1323–1325.

Haque, M. E., Negnevitsky, M., and Muttaqi, K. M. (2008). A Novel Control Strategy for a Variable Speed Wind Turbine with a Permanent Magnet Synchronous Generator. *IEEE Industry Applications Society Annual Meeting*.

Héctor Huerta. (2018). Doubly-fed induction generator control via integral high order sliding modes. *Control Engineering and Applied Informatics*, 20(1), 48-58.

Hong, C.-M., and Chen, C.-H. (2014). Intelligent control of a grid-connected wind-photovoltaic hybrid power systems. *International Journal of Electrical Power & Energy Systems*, 55, 554–561.

Hong, C.-M., Ou, T.-C., and Lu, K.-H. (2013). Development of intelligent MPPT (maximum power point tracking) control for a grid-connected hybrid power generation system. *Energy*, 50, 270–279.

Judewicz, M. G., Gonzalez, S. A., Echeverria, N. I., Fischer, J. R., and Carrica, D. O. (2016). Generalized Predictive Current Control (GPCC) for Grid-Tie Three-Phase Inverters. *IEEE Transactions on Industrial Electronics*, 63(7), 4475–4484.

Kadri, R., Gaubert, J.-P., and Champenois, G. (2011). An Improved Maximum Power Point Tracking for Photovoltaic Grid-Connected Inverter Based on Voltage-Oriented Control. *IEEE Transactions on Industrial Electronics*, 58(1), 66–75.

Kim, S.-K., Park, C. R., Kim, J.-S., and Lee, Y. I. (2014). A Stabilizing Model Predictive Controller for Voltage Regulation of a DC/DC Boost Converter. *IEEE Transactions on Control Systems Technology*, 22(5), 2016–2023.

Kouro, S., Cortes, P., Vargas, R., Ammann, U., and Rodriguez, J. (2009). Model Predictive Control—A Simple and Powerful Method to Control Power Converters. *IEEE Transactions on Industrial Electronics*, 56(6), 1826–1838.

Larrinaga, S. A., Vidal, M. A. R., Oyarbide, E., and Apraiz, J. R. T. (2007). Predictive Control Strategy for DC/AC Converters Based on Direct Power Control. *IEEE Transactions on Industrial Electronics*, 54(3), 1261–1271.

Lekouaghet, B., Boukabou, A., Lourci, N., and Bedrine, K. (2018). Control of PV grid connected systems using MPC technique and different inverter configuration models. *Electric Power Systems Research*, 154, 287–298.

Maiti, S., Chakraborty, C., and Sengupta, S. (2009). Simulation studies on model reference adaptive controller based speed estimation technique for the vector controlled permanent magnet synchronous motor drive. *Simulation Modelling Practice and Theory*, 17(4), 585–596.

Nauman, M., and Hasan, A. (2016). Efficient Implicit Model-Predictive Control of a Three-Phase Inverter With an Output LC Filter. *IEEE Transactions on Power Electronics*, 31(9), 6075–6078.

Panten, N., Hoffmann, N., and Fuchs, F. W. (2016). Finite Control Set Model Predictive Current Control for Grid-Connected Voltage-Source Converters With LCL Filters: A Study Based on Different State

Feedbacks. *IEEE Transactions on Power Electronics*, 31(7), 5189–5200.

Rezvani, A., Khalili, A., Mazareie, A., and Gandomkar, M. (2016). Modeling, control, and simulation of grid connected intelligent hybrid battery/photovoltaic system using new hybrid fuzzy-neural method. *ISA Transactions*, 63, 448–460.

Rodriguez, J., Kazmierkowski, M. P., Espinoza, J. R., Zanchetta, P., Abu-Rub, H., Young, H. A., and Rojas, C. A. (2013). State of the Art of Finite Control Set Model Predictive Control in Power Electronics. *IEEE Transactions on Industrial Informatics*, 9(2), 1003–1016.

Rodriguez, J., Pontt, J., Silva, C. A., Correa, P., Lezana, P., Cortes, P., and Ammann, U. (2007). Predictive Current Control of a Voltage Source Inverter. *IEEE Transactions on Industrial Electronics*, 54(1), 495–503.

Saad, N. H., El-Sattar, A. A., and Mansour, A. E.-A. M. (2017). A novel control strategy for grid connected hybrid renewable energy systems using improved particle swarm optimization. *Ain Shams Engineering Journal*.

Scoltock, J., Geyer, T., and Madawala, U. K. (2015). Model Predictive Direct Power Control for Grid-Connected NPC Converters. *IEEE Transactions on Industrial Electronics*, 62(9), 5319–5328.

Seul-Ki Kim, Jin-Hong Jeon, Chang-Hee Cho, Jong-Bo Ahn, and Sae-Hyuk Kwon. (2008). Dynamic Modeling and Control of a Grid-Connected Hybrid Generation System With Versatile Power Transfer. *IEEE Transactions on Industrial Electronics*, 55(4), 1677–1688.

Shtessel, Y., Taleb, M., and Plestan, F. (2012). A novel adaptive-gain supertwisting sliding mode controller: Methodology and application. *Automatica*, 48(5), 759–769.

Slotine JJ, Li W. (1991).Applied nonlinear control. London: Prentice- Hall, Inc.

Song, Z., Xia, C., and Liu, T. (2013). Predictive Current Control of Three-Phase Grid-Connected Converters With Constant Switching Frequency for Wind Energy Systems. *IEEE Transactions on Industrial Electronics*, 60(6), 2451–2464.

Tremblay, O., Dessaint, L.-A., and Dekkiche, A.-I. (2007). A Generic Battery Model for the Dynamic Simulation of Hybrid Electric Vehicles. 2007 *IEEE Vehicle Power and Propulsion Conference*.

Utkin V, Guldner J, Shi J (2009). Sliding mode control in electromechanical systems. *2nd ed. London: Taylor and Francis.*

Vazquez, S., Rodriguez, J., Rivera, M., Franquelo, L. G., and Norambuena, M. (2017). Model Predictive Control for Power Converters and Drives: Advances and Trends. *IEEE Transactions on Industrial Electronics*, 64(2), 935–947.

Zhang, Q., Min, R., Tong, Q., Zou, X., Liu, Z., and Shen, A. (2014). Sensorless Predictive Current Controlled DC–DC Converter With a Self-Correction Differential Current Observer. *IEEE Transactions on Industrial Electronics*, 61(12), 6747–6757.

APPENDICES

Appendix 1. Detail simulation parameters of the VSC.

Parameters	Values
DC-Link voltage (V_{dc})	660V
Capacitance of the DC link (C_{dc})	6000μF
Grid operating voltage	220V
Filter inductance (L)	6 mH
Grid frequency (f)	50Hz
Filter resistance (R)	0.01Ω
Sample Time (T_s)	50 μs